Sequence Analysis of Candidate Genes Involved in Causing Bone Deformities in Consanguineous Families

By

Rehmat Ullah Kakar

Department of Biochemistry

Faculty of Biological Sciences

Quaid-i-Azam University Islamabad, Pakistan

2024

Sequence Analysis of Candidate Genes Involved in Causing Bone Deformities in Consanguineous Families

A thesis submitted in partial fulfillment of the requirements for the degree of Master of Philosophy

in

Biochemistry/Molecular Biology

by

Rehmat Ullah Kakar

Department of Biochemistry

Faculty of Biological Sciences

Quaid-i-Azam University Islamabad, Pakistan,

2024

Dedicated to My parents, My uncle, and all family members,

Ghani khan BABA (late)

And

Ex-Senator Shaheed Usman LALA (late)

Declaration

I hereby declare that the work presented in this thesis is my effort and hard work. It is written and composed by me. No part of this thesis has been previously published or presented for any other degree or certificate.

Rehmat Ullah Kakar

Quaid-i-Azam University, Islamabad, PAKISTAN
Department of Biochemistry
Faculty of Biological Sciences

CERTIFICATE

This thesis, submitted by **Mr. Rehmat Ullah** to the Department of Biochemistry, Faculty of Biological Sciences, Quaid-i-Azam University, Islamabad, Pakistan, is accepted in its present form as satisfying the thesis requirement for the Degree of Master of Philosophy in Biochemistry/Molecular Biology.

Examination Committee:

1. **External Examiner:**   Signature:_____

2. **Supervisor:**   Signature:_____
   Dr. Imran Ullah

3. **Chairperson:**   Signature:_____
   Prof. Dr. Iram Murtaza

Dated:

ACKNOWLEDGMENTS

Table of Contents

LIST OF FIGURES

LIST OF TABLES

LIST OF ABBREVIATIONS

AD	Autosomal Dominant
AR	Autosomal Recessive
AMD	Acromesomelic Dysplasia
AER	Apical Ectodermal Ridge
BBS	Bardet-beidl Syndrome
BCC	Basal Cell Carcinoma
CED	Camaurati Engelman Disease
CFAP	Cilia and Flagella Associated Protein
CNV	Copy Number Variation
CRD	Cysteine-rich Domain
CRJS	Curry–Jones syndrome
CZIB	CXXC Zinc Binding motif Protein
DACH1	Dachshund Family Transcription Factor 1
DNA	Deoxyribonuclease
EB	Elution Buffer
ECD	Extracellular Domain
EDTA	Ethylene Diamine Tetraacetate
EtBr	Ethidium Bromide
EVS	Ellis-Van Crevald Syndrome
FGF	Fibroblast growing factor
GATK	Genome Analysis Tool kit
GCPS	Greig Cephalo-Polysyndactyly Syndrome
GSD	Genetic Skeletal Dysplasia
HEC	Higher Education Commission
HGMD	Human Genome Mutation Database

HOX	Homeobox gene
IFSSH	The International Federation of Societies

	for Surgery of Hand
IQCE	IQ Motif containing E
IRB	Institutional Review Board
LMBR1	Limb Development Membrane Protein 1
MB	Medulloblastoma
MSC	Mesenchymal stem cell
OD	Optical Density
PAP	Postaxial Polydactyly
PAP-A	Postaxial Polydactyly Type A
PAP-B	Postaxial Polydactyly Type B
PCR	Polymerase Chain Reaction
PPD	Preaxial Polydactyly
PHS	Pallister-Hall Syndrome
Rpm	Rotation Per Minute
SHFM	Split Hand and Foot Malformation
SD	Syndactyly
SMO	Smoothened
SNV	Single Nucleotide Variant
TBE	Tris-Borate EDTA
TE	Tris EDTA Buffer
TGF- β	Transforming Growth Factor Beta
TMPPE	Transmembrane Protein with metallophosphoterase domain

TPT	Tri-phalangeal Thumb
RA	Retinoic Acid
GLI3	Gli Family Zinc Finger 3
WB	Wash Buffer
WES	Whole Exome Sequencing

WNT	Wingless-type MMTV integration site family
YCGA	Yale Centre for Genome Analysis
ZNF	Zinc Finger Protein
ZPA	Zone of the Polarising Activity

ABSTRACT

Polydactyly is a genetic limb disorder characterized by the presence of an extra digit. Postaxial polydactyly (PAP) refers to one or more additional digits at the ulnar or fibular side of the hand or foot respectively. Syndactyly stands out as one of the most diverse developmental deformities documented in medical literature. Various combinations exist where adjacent fingers or toes remain connected by a web, allowing for unilateral or bilateral occurrences, as well as symmetrical or asymmetrical manifestations. The study presented in this dissertation was aimed to hunt down the disease-causing genes and mutations involved in the pathogenesis of distinctive skeletal disorders in four families (A, B).

Family A showing an autosomal recessive or X-linked recessive inheritance pattern in the consanguineous family was followed for WES. Clinical features observed in affected individuals of family A included Postaxial polydactyly type A. The WES followed by Sanger sequencing was performed to identify the potential disease-causing variant. Two variants of two genes located on X chromosome (*WDR13* Xp11.23 exon2:c.C29T and *MED12* Xq13.1 exon41:c.G5873C) and one variant of a gene (*MEOX2* 7P21.2 Exon1:c .225_230del) located on the autosomal chromosome were shortlisted. Sanger sequencing data does not show any pathogenic variant in these genes However, one affected member of the family showed a pathogenic variant and DNA Sanger sequencing of parents and other normal siblings will be further investigated to confirm segregation.

In family B, clinical features observed in the patients included cutaneous syndactyly in the 4th and 5th toes with no other symptoms showing isolated syndactyly. Homozygosity mapping was tested for previously reported genes *LRP4* (11p11.2), *BHLHA9* (17p13.3), *LMBR1* (7q36.3), *CKAP2L* (2q14.1), *CHST1* (11p11.2), *SMO* (7q32.1), *LAMA2* (6q22.33), *SOST* (17q21.31), *PAX3* (2q36.1), *EDNRB* (13q22.3) and *RAB23* (6p12.1-p11.2). None of the listed genes showed any linkage. However, one STS marker of *HOXD12* (2q31.1) showed linkage. One exon of *HOXD12* was sequenced which did not show any pathogenic variant so, the remaining exons will be sequenced. If no pathogenic variant is found, then family B will be subjected to whole exome sequencing and there might be a novel gene involved in causing disease in this family.

INTRODUCTION

Skeleton System

The human skeleton is a complex and remarkable structure that serves as the framework for the human body. It is a network of bones, cartilage, ligaments, joints, and tendons (Shipman *et al*., 1985). The primary role of the skeleton is to provide structural support and proper shape to the body (Poduval, 2015). It also plays many other vital roles in our body i.e., to protect vital organs (brain, heart, lungs) from injury, involved in body movement and locomotion, reservoir for minerals (particularly calcium and phosphorus), and production of hematopoietic cells (Gentry *et al*., 1998)

The human skeletal system consists of hardened, mineralized components embedded within soft tissues. In the developmental stages of vertebrates, versatile mesenchymal cells, originating from both ectoderm and mesoderm, move to specific areas of the body, initiating the process known as Skeletogenesis (Byers and Steniner, 1992). These embryonic cells then undergo further specialization, resulting in the formation of three distinct cell types: chondrocytes, osteoclasts, and osteoblasts. Skeletogenic cells use two distinct processes i.e. intramembranous and endochondral ossification to initiate osteogenesis, the process that results in the formation of bones, after this differentiation. Long bones grow because of endochondral ossification, whereas the bones of the craniofacial skeleton and some clavicle parts are formed via intramembranous ossification (Anat Embryol, 2004).

Bone Formation

Bone is a highly specific component and the most important connective tissue of the skeleton. It plays a crucial function in mobility, soft tissue support, defense, mineral storage, and hosting microbes (Kini and Nandeesh, 2012; Florencio-Silva *et al*., 2015). The development of woven bone occurs as a result of the incorporation of collagenous mesenchymal tissue into the bone structure. which represents an early, primitive stage characterized by randomly arranged collagen fibers. Subsequently, this woven bone undergoes remodeling to transform into mature lamellar bone. Ongoing maintenance and remodeling of lamellar bone are carried out by osteoclasts

and osteoblasts (Setiawan and Rahardjo, 2019). Bones come in various types based on their shapes. Flat bones, for instance, originate from the membrane (membrane model), while sesamoid bones develop from tendons (tendon model) (Waugh and Grant, 2018). Hyaline cartilage (cartilage model) serves as the precursor for the formation of irregular bones, long bones, and short bones. Following the establishment of the cartilage model, osteoblasts, through the process of endochondral ossification, replace the cartilage with bone matrix (Robson and Syndercombe, 2018).

Structural Segmentation of Human Skeleton

The human skeleton is divided into many parts according to its different structural segmentation. It is comprised of 206 bones (which have 126 appendicular, 74 axial, and 6 ossicle bones) cartilages, and joints (Ahmad *et al*., 2022).

Bones have been divided into four subtypes:

Long Bones

The term "long bones" refers to those bones whose length exceeds their width, and which have a lengthy base with two considerable ends. Long bones are primarily made of compact bone, although they can also have a large quantity of spongy bone toward their extremities. Long bones include those found in the arm, forearm, leg, and thigh (Taichman, 2005; Ahmed *et al*., 2022).

Short bones

Short bones are essentially cube shaped, with almost equal horizontal as well as vertical lengths. These are mostly made up of spongy bone and a thin covering of compact bone coats them. Ankle and wrist bones are considered as short bones.

Flat Bones

Thin, flattened, and typically bent bones are called flat bones. Bones of cranium are usually flat.

Irregular Bones

These are predominantly composed of spongy bone and a thin covering of compact bone is present beneath them. There are projections, smooth facets, depressions, and

holes. Examples of irregular bones include the vertebrae and certain bones in the skull.

Skeletogenesis

The formation of the skeleton, known as skeletogenesis, is a crucial process in the growth and development of vertebrates which initiates with the proliferation of multipotent mesenchymal cells during the early embryonic phase (Crombrugghe *et al.,* 2001). It involves the ectoderm differentiation into the neural tube, the mesoderm is differentiated into notochord and lateral-plate mesoderm and para-axial mesoderm development into various other skeletal elements. The neural crest, a densely populated group of cells derived from the neural tube, undergoes epithelial-mesenchymal transformation (EMT), giving rise to various cell types, including neuronal, melanocyte, and skeletogenic cells. Subsequently, these skeletogenic cells develop into the craniofacial skeleton. The lateral plate mesoderm differentiates into the appendicular skeleton (limb bones), and the sternum (part of the axial skeleton). The para-axial mesoderm develops into dermo-myotomes and sclerotomes, laying the foundation for the axial skeleton (Lefebvre and Bhattaram, 2010; Usami *et al*., 2015).

Skeletogenesis is achieved by two processes i.e. intra-membranous ossification and endochondral ossification respectively (Baat *et al*., 2005; Spranger, 2006). Endochondral ossification involves hypertrophy, degradation, and eventual transformation into bone, wherein chondrocytes are replaced by osteoblasts. This process results in the formation of a mature bone, occurring through a sequence of prenatal and postnatal growth stages (Kornak and Mundlos, 2003). On the other hand, intra-membranous ossification directly converts mesenchymal stem cells into osteoblast cells via direct differentiation (Savarirayan and Rimoin, 2002).

Appendicular skeleton

One of the two main bone groups in the body, the appendicular-skeleton differs from the axial-skeleton. It includes the bones of feet and hands, pelvic bones, shoulder girdle and upper and lower extremities. To enable the transfer of mechanical loads between the axial and appendicular skeletons, the shoulder girdle and pelvis are essential connecting points (Docherty, 2007; Anderson *et al*., 2018). The lateral plate

mesoderm forms the limb buds that eventually become the appendicular or limb skeleton through interactions with the underlying ectoderm. Inside the growing limb bud, the progress zone undergoes differentiation into dorsoventral, proximodistal, and anteroposterior axes, each regulated by specific signaling molecules. WNT7A [MIM#276820] and LMX-1 [MIM#601412] genes play a significant role in controlling dorsoventral patterning. Proximodistal extension is managed by the apical ectoderm [AER], which utilizes FGF-signaling to interact with underlying mesenchymal cells. Meanwhile, in Zone of Polarizing Activity center (ZPA), Sonic Hedgehog (SHH) and Bone Morphogenetic Proteins (BMPs) actively contribute to establishing the anteroposterior polarity of developing limbs (Pizette *et al*., 2001; Altabef and Tickle, 2002). Mutations in the SHH gene or its downstream target genes lead to both syndromic and non-syndromic limb abnormalities, including polydactyly, brachydactyly, synpolydactyly, and ectrodactyly (Kornak and Mundlos, 2003).

Axial skeleton

The axial-skeleton serves as the body's center axis. It consists of approximately 80 bones distributed across various segments of the vertical skeleton. These bones collectively create the "Cervicothoracic junction," establishing essential functional connections between the thorax, spine, and shoulder (Clarke, 2008). The essential components of the axial skeleton encompass the bones of the skull, rib cage, vertebral column, interconnected joints, and ligaments in the neck, trunk, and tail regions. Its main function involves offering support and safeguarding the head and spinal cord, while also providing anchorage to skeletal muscles to ensure stability and facilitate movement (Mallo *et al*., 2020).

Malformations of the axial skeleton are typically categorized as spondylocostal dysostosis (SCDs). Clinically it is characterized by a range of defects involving the vertebrae and ribs. These may encompass vertebral and rib fusion, truncal dwarfism, and occasionally the presence of syndactyly and polydactyly. SCDs are attributed to mutations in the RIPPLY2 gene (MIM#609891), LFNG gene (MIM#602576), MESP2 gene (MIM#605195), HES7 gene (MIM#608059), DLL3 gene (MIM#602768), and TBX6 gene (MIM#602427). SCDs result from homozygous loss-of-function (LOF) variants in these genes, except for TBX6, which follows a dominant inheritance pattern (Sparrow *et al*., 2013).

Limb development

Appendages known as limbs serve crucial functions in communication, locomotion, and various intricate processes. The intricate shape and positioning of bones and joints in the vertebrate limb skeleton result from a complex interplay of multiple elements during its formation (Waldmann *et al*., 2022). Limb development unfolds along three axes, each governed by genetic signals prompted by the patterning process. They encompass "proximal–distal" (shoulder-finger), "anterior–posterior" (thumb-little finger), and "dorsal–ventral" (the back-palm) (Ahmad *et al*., 2022).

When the lateral plate undergoes an epithelial-mesenchymal transition brought on by FGF signals from the ectoderm, limb development begins (Tabin and Gross, 2014). A complex gene regulatory network (GRN) that is impacted by transcription factors, signaling pathways, and epigenetic modifiers controls the development of vertebrate limbs. Leg growth initiates at the lateral plate mesoderm, where mesenchymal precursors form a small bud enveloped in an ectodermal layer. Retinoic acid and Wnt signaling cause limb induction (Ng *et al*., 2002). The transcription factors TBX5 and TP63 increase the expression of fibroblast growth factor 10 (FGF10) in the mesenchyme and FGF8 in the outer ectoderm, which starts the process of growth at the apical ectodermal ridge (AER) (Agarwal *et al*., 2003).

Homeobox genes like HOXA11, HOXA13, and HOXD13 contribute to the initial patterning of cartilage in the development of the limbs. The HOX code contributes to the positioning of the limb field in vertebrates. The Apical Ectodermal Ridge (AER), Zone of the Polarising Activity (ZPA), and dorsal ectoderm are key players in regulating a patterning in the anteroposterior (A/P) axis, proximal to distal projection, and establishing dorsoventral polarity respectively (Hong *et al*., 2012).

Digital development

After digits arise from a single chondrogenic plate, the digit rays are shaped by the autopod plate. After 44–46 days of fertilization, interdigital tissues divide these rays. (Cole *et al*., 2009). The undifferentiated limb Mesenchymal Stem Cells (MSCs) function as a reservoir of progenitor cells that can subsequently transform into bone,

cartilage, ligaments, dermis, and tendons (Marin-Llera *et al*., 2019). Expression of FGFs and WNT helps sustain the pools of progenitor cells and simultaneously prevent cell death and cell differentiation. This conserves reservoir of undifferentiated MSCs (Yu and Ornitz, 2008; Mariani *et al*., 2008;) and triggers the of Sox9 expression (Kumar and Lassar, 2014). Initiation of chondrogenesis occurs when pool of progenitor cell expresses Sox9, leading to the expression of Sox6, Sox5, type II collagen, sulfated proteogylcans and aggrecan (Montero and Hurle, 2007; Lefebvre, 2019). The Sox9 expression in mesenchymal cells facilitates both aggregation of cell and the synthesis of cartilage-forming proteins, including type II collagen, aggrecan, and sulfated proteoglycans (Marin-Llera *et al*., 2019). While FGF and Wnt govern the ectoderm to determine the size of the developing phalanges, BMP 2, 4, and 7 control the mesoderm (Guero, 2018). Suppression of the interdigital mesenchyme using TGF-ß and/or Activin with BMP inhibits the gene Sox9, leading to a delay in chondrogenesis and areas where cartilage formation is deficient (Montero *et al*., 2008). In the limb buds from undifferentiated mesenchymal cells the early removal of Sox9 resulted in a lack of cartilage differentiation, leading to the digit-formation inhibition (Chimal Monroy *et al*., 2011).

GLI3R, located on anterior region of the autopod is involved in the identification of the thumb (Guero, 2018). Forearm radial side and the thumb's radial edge are both impacted by TBX5 (Oberg, 2014). Once the identities of the digits have been established, each primordium starts to elongate distally before the phalanges formation (Hu and He, 2008). The distal-phalanx initially takes the form of a cartilaginous skeleton, along with ossification commencing at distal ends. Bambi, MSX1 and STP8 are expressed when nail growth starts on the distal side at each end of the terminal phalanx. This expression maintains the potential for fingertip regeneration (Guero, 2018). Following the digits elongation, they are formed into metacarpals and metatarsals and phalanges. Like the elongation process, digits segmentation follows specific order. The first digit undergoes segmentation twice, and the other digits experience segmentation three-times (Mundlos and Stricker, 2011).

Skeletal Dysplasia

A group of rare and varied disorders, collectively known as skeletal dysplasia (SD) often referred to as "osteochondrodysplasia," has a notable impact on the skeleton. These conditions are characterized by abnormalities in cartilage and bone formation, leading to irregularities in bone length, shape, or density causing disrupted skeletal development (Namba, 2010; Marzin and Daire, 2020).

Genetic skeletal disorders are categorized into nonsyndromic (isolated) or syndromic (complex syndromes) forms and are inherited in autosomal dominant, autosomal recessive, X-linked, or de novo patterns (Abbas *et al*., 2023). The "Nosology of Genetic Skeletal Disorders" underwent its 11th revision in 2023. In the latest classification, 552 genes are identified to be responsible for 771 well-characterized skeletal disorders, each with a unique MIM number (available in its online version OMIM). These skeletal disorders are now organized into 41 different groups, compared to the previous revision which had 42 groups. Several modifications and updates were introduced in the current nosology (Unger *et al.,* 2023).

Skeletal dysplasia is divided into three main types: Osteochondrodysplasia (OCD) or skeletal dysplasia (SD), osteodystrophies, and dysostoses constitute the three primary categories of heritable skeletal abnormalities (Cavalcanti *et al*., 2020). Skeletal dysplasia (SD) or osteochondrodysplasia (OCD) refers to disorders characterized by innate defects in bone or cartilage, affecting multiple bones primarily due to altered transcription factors or signal transducing genes. Examples among them include osteogenesis imperfecta, Split Hand and Foot malformations (SHFM), and polydactyly. Osteodystrophies involve metabolic or nutritional disorders that are unrelated to bone, such as rickets, while dysostoses focus on specific bone abnormalities, including disruptions in certain bones during the first six weeks of life (Cavalcanti *et al*., 2020).

A diverse array of signaling cascades, including TGF-β, FGF, Notch, BMP, WNT, and Hedgehog pathways, play vital roles in the development of the human skeletal system. Any primary or secondary disruption of these mechanisms or pathways can lead to osteochondrodysplasias. For instance, mutations in TGF-β1, a member of the transforming growth factor (TGF-β) signaling cascade, result in Camurati-Engelmann

Disease (CED). Additionally, mutations in SOST, a member of the WNT pathway, are linked to sclerosteosis. Chondrodysplasias such as hypochondroplasia, thanatophoric dysplasias, and achondroplasias can occur due to mutations in FGFR3, a member of the FGF signaling pathway (Baldridge *et al*.,2010).

Polydactyly

The appearance of extra digits in the hands and feet is a characteristic of polydactyly (PD), the most frequent limb abnormality.

This disorder can include as a component of many defects (syndromic) or as an inheritable independent disorder (non-syndromic). The malformation known as polydactyly is very diverse and tends to affect the right-hand more often than the left hand. Furthermore, left foot is typically more affected than the right, and upper limbs are more commonly affected than the lower limbs. (Malik *et al*., 2014). The development of polydactyly is attributed to the abnormal patterning of the anterior-posterior (A-P) axis during appendage development.

Numerous mutations can result in polydactyly; these mutations can happen in the genic region (coding region) or in a "cis-regulatory" element that controls the expression of a particular gene (Niha, 2017). According to studies conducted in the United States, Black women are 22 times more likely than White women to have polydactyly, while Black males are 10 times more likely than White men to have it. In comparison to Black females, who have polydactyly at a rate of 11.1/1000, White males experience it at a rate of 2.3 per 1000, Black males at 13.5 per 1000, and White females at 0.6 per 1000. (Finley *et al*., 1994).

Classification of Polydactyly

Polydactyly is broadly classified into syndromic and non-syndromic types. Pre-axial polydactyly (PPD) is characterized by the presence of an extra digit on the radial side of the hand (thumb side) or tibial part of the foot (first toe), aligned with the anterior to median axis of the limb. On the other hand, post-axial polydactyly (PAP) is identified by an additional digit attached to the fifth finger or toe, forming the ulna aspect of the hand and fibular part of the foot, respectively, positioned along the posterior axis to the median axis of the limbs (Lange and Muller, 2017).

Syndromic polydactyly

Syndromic polydactyly has demonstrated its prevalence in numerous ailments along with the multitude of symptoms of other syndromes. 221 syndromic polydactylies and 120 syndromic oligodactyly disorders are being reported by the London Dysmorphology database (Ahmad *et al*., 2023). ‗8659' entries appear as ‗Syndromic Polydactyly' in the online OMIM database (https://www.omim.org/). The most reported digit abnormalities are Ellis Van Crevald Syndrome (OMIM 225500), Pallister-Hall Syndrome (OMIM 146510), Bardet-Biedl Syndrome (OMIM 617119), and Greig Cephalopolysyndactyly Syndrome (OMIM175700) (Ahmad *et al*., 2023).

Non-Syndromic Polydactyly

Pre-axial polydactyly (radial), central polydactyly (axial), and postaxial polydactyly (ulnar) are three broadly distinguished main sub-types of non-syndromic polydactyly (Umair *et al*., 2018). Various types and sub-types of non-syndromic polydactyly are discussed below:

Pre-axial polydactyly

Preaxial polydactyly (PPD) refers to the presence of an additional digit next to the first digit on the radial side of the hand (thumb) or on the tibial side of the foot (toe). After post-axial polydactyly (PAP), PPD stands as one of the most common congenital hand abnormalities, with an occurrence rate ranging from 0.08 to 1.4 per 1000 live births (Manske *et al*., 2018).

Pre-axial Polydactyly Type 1 (PPD1)

The most common type of polydactyly is thumb polydactyly, which is a biphalangeal thumb duplication (MIM 174400). In a bilateral form, upper limbs are more afflicted than lower limbs, and right-hand PPD is more common than left-hand PPD. It is typically inherited in a unilateral form (Malik *et al*., 2014). Pre-axial type 1 polydactyly is caused by sequence mutations in the zone of polarizing activity (ZPA) regulatory sequence (ZRS), which is housed within the sonic hedgehog (SHH) enhancer. (Perez-Lopez *et al*., 2018).

Pre-axial Polydactyly Type 2 (PPD2)

PPD2 (OMIM: 174500) depicts the triphalangeal thumb i.e., three phalanges with or without duplicated thumb with autosomal dominant inheritance and 7q36.3 locus (Umair *et al*., 2018; Ahmad *et al*., 2023) due to which it is also called as ─triphalangeal thumb polydactyly (TTP)". PPD2 is found to be functionally associated with the gene locus of LMBR1 specifically in the intron 5 comprising the cis-regulatory sequence (Lettice *et al.,* 2003).

Pre-axial polydactyly type 3 (PPD3)

PPD type 3 (OMIM 174600) is also recognized as index finger polydactyly wherein the index finger is typically duplicated. It distinguishes itself from PPD-2 as, in type 3, the thumb is replaced with one or two triphalangeal digits, and the metacarpal exhibits a distal epiphysis. This condition often follows autosomal dominant inheritance. The responsible gene for PPD type 3 is currently unknown (Kyriazis *et al*., 2023). The additional digit typically exhibits significant angulation or radial deviation, and the normal digit may show varying degrees of deviation towards the ulnar side.

Pre-axial polydactyly type 4 (PPD4)

The duplication of the mildest degree in combination with the webbed or connected fingers or toes, is seen in PPD4 (OMIM: 174700), commonly also known as polysyndactyly (Umair *et al*., 2018; Ahmad *et al*., 2023). This PPD type is located at p14.1 of chromosome 7 in humans with the autosomal dominant inheritance corresponding to the GLI3 gene locus.

Table 1.1: molecular genetics of different polydactyly types

OMIM ID	Phenotype	Inheritance	Genes	No. of mutations	Locus
174400	PPD1	AD	U	-	U
174500	PPD2	AD	ZRS/SHH	2	7q36
174600	PPD3	AD	U	-	U
174700	PPD4	AD	GLI3	1	7p14.1

AD autosomal dominant; U unknown

Mexoaxial polydactyly

Mesoaxial polydactyly also known as central polydactyly is a comparatively uncommon form representing only 5-15% of all polydactylies. This condition impacts the mid digits of the hands or feet and manifests as a concealed duplication with tissue mass located in the center of the hand, often presenting as synonychia or apparent syndactyly (Bubshait and Dalal, 2022).

Type I Duplications

Duplications of type I lack an osseous or ligamentous link to the neighboring digit (Umair *et al*., 2018).

Type II Duplications

Duplications of type II exhibit ligamentous and soft tissue characteristics within the duplicated digit, sharing a phalanx, bifid metacarpal, or joint with the adjacent digit. Simultaneous syndactyly may or may not be present (Umair *et al*., 2018).

Type III Duplications

Duplication of type III has a completely formed metacarpal in central polydactyly. Fourth digits are most frequently duplicated, and the deformity is typically bilateral with the dominant inheritance pattern (Umair *et al*., 2018).

Post-axial polydactyly

Post-axial polydactyly (PAP), also known as ulnar polydactyly, is prevalent, representing 77-87% of all cases. It is typically characterized by the presence of extra digits on the ulnar side of the hand along the fifth finger. The spectrum of additional digits ranges from basic skin tags to fully formed, functional digits, with most of them developing from soft tissue components (Ahmed *et al*., 2023). Its prevalence at birth is approximately 1–2 per 1000, with variations observed among different ethnic groups (Zhou *et al*., 2004). PAP is subdivided into two categories depending on the duplicated extra digit(s); Postaxial Type A (PAP-A), and Postaxial Type B (PAP-B). Both types differ in their prevalence, inheritance pattern, and severity (Verma and ElHarouni, 2015).

Post-axial polydactyly type A (PAPA)

In postaxial polydactyly type-A (PAP-A), a fully formed additional digit, complete with bone, develops at the 5th/6th metacarpal. This duplicated digit consists of one to three bony elements and features a fully developed nail. While the extra digit is non-functional, it may present challenges in normal daily activities. Type-A inheritance can occur in either an autosomal dominant or an autosomal recessive manner. In the literature, PAP-A is further categorized into 11 subtypes (PAP-A1 to PAP-A11) based on genetic considerations (Umair *et al*., 2018).

Post-axial Polydactyly Type A-1 (PAPA1)

The fifth metacarpal has an effective additional finger and is caused by heterozygous variation in the GLI3 gene (OMIM 165240) on chromosome 7p14.1 that is autosomal dominantly inherited (Umair *et al*., 2018; Rahim *et al*., 2020). Genetic testing revealed a heterozygous variation in the GLI3 gene that is expected to cause premature termination and may contribute to nonsense-mediated mRNA degradation. There have been 330 GLI3 genetic variations documented that are linked to different skeletal disorders (Furniss *et al*., 2007; Ahmad *et al*., 2023).

Post-axial Polydactyly Type A-2 (PAPA2)

Postaxial Polydactyly A type 2 (OMIM 602085) is inherited in either unilateral or bilateral isolated form with clinical features overlapping with PAP-A1. The causative gene is not discovered yet (Ahmad *et al.,* 2023), but located on 13q21-q32 chromosome (Akarsu *et al*., 1997).

Post-axial Polydactyly Type A-3 (PAPA3)

Post-axial Polydactyly A type 3 (OMIM 607324) was discovered for the first time in a Chinese family in a dominant form with characteristics of PAP type A as well as B. The affected members of the family exhibited fully developed and functional bilateral PAP but had different expression patterns (Zhao *et al*., 2002). The causative gene for PAP-A3 is still unknown but caused by mutation at chromosomal location 19p13.2p13.1 (Ahmad *et al*., 2023).

Post-axial polydactyly type A4 (PAPA4)

Postaxial Polydactyly A type 4 (OMIM 608562), mapped on chromosome 7q22, was determined in a large Dutch family. PAP-A4 exhibits an autosomal dominant inheritance pattern. PAP-A4 is characterized by PAP and in some cases, with partially cutaneous syndactyly. The expression of polydactyly and syndactyly is variable in PAP-A4, suggesting that these phenotypes have substantial penetrance and genetic heterogeneity (Galjaard *et al.,* 2003). The responsible gene is still unknown.

Post-axial polydactyly type A5 (PAPA5)

Bilateral postaxial polydactyly with the AR inheritance is the clinical feature of PAPA5 (OMIM:263450), (Ahmad *et al*., 2023). A Pakistani family having brother and sister pairs bearing bilateral PAP at both the upper as well as lower extremities was the first to report PAPA5 (Umm-e-kalsoom *et al*., 2012). The mapping of PAPA5 was determined at 13q13.3-q21 between D13S1288 and D13S632 markers, spanning a region of 17.87cM, utilizing a genome-wide scan with highly polymorphic microsatellite markers of a physical map providing the maximum LOD score of 3.84 (Umm-e-Kalsoom *et al*., 2012).

Post-axial polydactyly type A6 (PAPA6)

Post-axial polydactyly A type 6 (OMIM 615226) was initially mapped on chromosome 4p16.3 in the closely related Pakistani family. It was reported as a second locus for PAP-A with an autosomal recessive inheritance mode. The affected individuals had a bilateral, completely developed 5th finger in their hands as well as in their feet with either radial or ulnar deviation in different members and, in some cases, had a duplicated distal phalanx. No other additional symptoms were observed in affected family members which indicated isolated PAP. The WES of the affected family discovered a missense homozygous mutation in ZNF141 (OMIM 615226) gene (Kalsoom *et al*., 2013).

Post-axial polydactyly type A7 (PAPA7)

Postaxial polydactyly (PAP) limited to lower limbs, accompanied by well-developed nails, and inherited in a recessive (AR) manner, characterizes PAPA7 (OMIM: 617642). The IQCE gene, which encodes 695 amino acids across 22 exons in the

7p22.3 locus, harbors a homozygous splice acceptor site mutation (c.395>1G-A). This mutation is entirely co-segregated with a Pakistani consanguineous family exhibiting postaxial polydactyly traits, as confirmed through whole exome sequencing (WES) and minigene assay (Umair *et al.*, 2017).

Post-axial polydactyly type A8 (PAPA8)

Palencia-campos *et al.*, 2017 confirmed the correlation of the three unrelated families comprising biallelic homozygous nonsense variations in *GLI1* gene (NM:165220) with the PAPA8 (OMIM: 618123). Affected individuals were observed with additional features like postaxial polydactyly, atrial septal abnormalities, and minor nail dysplasias, in conjunction with short stature having AR pattern, which overlapped with the phenotypes of Ellis-van Creveld syndrome (EvC) brought on by the reduced hedgehog signaling to correlate with the GLI1 dosage mutation effect (Palencia-campos et al., 2017).

Post-axial polydactyly type A9 (PAPA9)

Non-syndromic post-axial polydactyly in the extremities integrated with recessive inheritance generates the clinical features of PAPA9 (OMIM: 618219) (Ahmad *et al.*, 2023). The FAM92A gene (NM: 618219) harbors a homozygous nonsense variation [c.478C>T, p.(Arg160*)] on chromosome 8q21.13-q24.12 found to be exhibiting PAPA9 in a Pakistani consanguineous family of three affected siblings (Schrauwen *et al.*, 2019).

Post-axial polydactyly type A10 (PAPA10)

Postaxial Polydactyly A type 10 (OMIM 618498) was found in two parentally linked Pakistani families, exhibiting bilateral polydactyly in hands as well as feet with varying metatarsal size and clinodactyly in some members. It is inherited as an autosomal recessive condition, caused by a mutation in KIAA0825 (OMIM 617226) gene located on chromosome 5q15 (Ullah *et al.*, 2019).

Post-axial polydactyly type A11 (PAPA11)

A non-syndromic recessive disorder called PAPA11 has symptoms like PAP in the upper as well as lower limbs along with the syndactyly in the middle toes (Ahmad *et*

al., 2023). Recent research has linked PAPA11 in a single Pakistani family to a biallelic missense mutation in the Dachshund homolog 1 gene (DACH1) (NM: 080760) on 13q21.33 chromosome (c.563>A, p. Cys188Tyr) with normal parents with no skeletal abnormalities (Umair *et al*., 2021).

Table 1.2: PAP Classification

Phenotype	OMIM ID	Locus	Genes	Inheritance
PAP1	174200	7p14.1	GLI3	AD
PAP2	602085	13q21-q32	U	AD
PAP3	607324	19p13.1-p13.2	U	AD
PAP4	608562	7q22	U	AD
PAP5	263450	13q13.3-q21	U	AR
PAP6	615226	4p16.3	ZNF141	AR
PAP7	617642	7p22.3	IQCE	AR
PAP8	618123	12q13.3	GLI1	AR
PAP9	618219	8q22.1	FAM92A	AR
PAP10	618498	5q15	KIAA0825	AR
PAP11	603803	13q21.33	DACH1	AR

 U: unknown, AD: autosomal dominant, AR: autosomal recessive

Post- axial polydactyly type B (PAPB)

This form of polydactyly is more prevalent. It often manifests as a skin extension, ranging from a minor protuberance to a spine-like outgrowth on the ulnar side of the fifth finger. Alternatively, it may appear as a nubbin-like structure, referred to as a "pedunculated postminimus," typically measuring 2–3 cm in length and often having a nail (Castilla *et al*., 1973).

A vestigial 6th finger is present in PAP-B affected individuals, at the base of the phalanx and metacarpal/metatarsal of hand/feet respectively. The additional finger is much smaller than the 5th finger and is present as a sac of tissue with a single phalanx and no bone and nail which can be easily removed by surgery (Holmes *et al*., 2018).

Mirror image polydactyly (MIP)

Duplication of posterior digits occurs in MIP (MIM135750), where the posterior digits completely replace the anterior digits in reverse order. One of the MIP phenotypes is caused by mutations in the MIPOL1 gene, which is located at chromosome 14q13 (MIM 606850) (Kondoh *et al*.,2002). Mutations in the PITX1 gene (MIM602149) have also been linked to MIP-related deformities of the lower limbs (Klopocki *et al*., 2012).

Syndactyly

Syndactyly (SD) is a diverse limb deformity characterized by the fusion of skin or bones between adjacent fingers and/or toes. It is relatively common; it has prevalence of 3-10 per 10,000 births. It is observed in males about twice as often as in females, which is explained by their incomplete penetrance behavior (Malik, 2012). Eight genes are associated with causing non-syndromic syndactyly to have been identified, including HOXD13 (MIM#186300), FBLN1 (MIM#608180), LRP4 (MIM#212780), GJA1 (MIM#186100), LMBR1/ZRS (MIM#186200), FGF16 (MIM#309630) and GREM1-FMN1. Potential genes implicated in triggering syndactyly also include semaphorin-3D (SEMA3D) and aldehyde dehydrogenase-1 family member A2 (ALDH1A2) (Elsner *et al*., 2021).

Classification of syndactyly

Syndactyly type I (SD1)

The isolated form SD1 (MIM 185900) inherits autosomal dominant manner. The phenotypical features of SD1 include the partial or total webbing of the second and third toes and the third and fourth fingers, as well as the association of bone fusion with this disorder. (Bosse *et al*., 2010).

It is further divided in four sub-types:

Syndactyly type I-a

SD1-a, (MIM 609815) also called Weidenreich type contains cutaneous fusion of the 2nd and 3rd toes without having hand deformities. Toes are rarely affected, and the phenotype is usually consistent in both feet (Malik *et al*., 2014).

Syndactyly type I-b

SD1-b (MIM 185900), also referred to as the Lueken type, represents the second most common variant of SD1. Clinical characteristics involve bilateral cutaneous fusion of the 3rd and 4th fingers, along with the fusion of the 2nd and 3rd toes (Ahmad *et al*., 2022).

Syndactyly type I-c

SD1-c, also known as the "Montagu type", manifests as syndactyly between the 3rd and 4th digits. Phenotypically it has features of unilateral or bilateral both cutaneous or bony webbing of the 3rd and 4th digits, with occasional webbing of the 4th and 5th digits, but without the involvement of the feet (Ghadami *et al*., 2001).

Syndactyly type I-d

SD1-d depicts bilateral cutaneous webbing of fourth and fifth toes and it is the second most common type of isolated webbing of toes having frequency of 0.22 in 10000 subjects (Malik *et al*., 2014).

Syndactyly type 2 (SD2)

Clinically and genetically, SD2 (MIM 185900) is one of the most varied forms. The third and fourth fingers and the second and third toes have fused together, either cutaneously or bonyly. Frequently, it entails the partial or total replication of a digital ray inside the syndactylous network. (Malik *et al*., 2014). This form of syndactyly is the second most prevalent, and it is linked with additional phenotypes like clinodactyly of the 5th digit, camptodactyly and brachydactyly (Ahmad *et al*., 2022).

Syndactyly type 3 (SD3)

SD3 (MIM 186100), sometimes referred to as Johnston-Kirby type or small ring syndactyly, is characterized by the presence of an underdeveloped middle phalanx in

the fifth finger with medially fused nails of the syndactylous fingers, as well as bilateral and/or fused distal phalanges (Malik, 2012).

Syndactyly type 4 (SD4)

SD4 (MIM 186200), known as Haas type syndactyly with a prevalence of 1 in 300,000, inherits an autosomal dominant form. Phenotypically there is complete cutaneous fusion of all fingers with the presence of extra digital pre- or postaxial ray(s) in the web. There is the entirely or partially fusion of nails. The fingers have a limited flexion, and cup shape appearance of the hand is due to the union of contiguous fingers. Phalanges may fuse as a conglomerate mass of bones however metacarpal synostosis is absent (Malik *et al*., 2014).

Syndactyly type 5 (SD5)

SD5 (MIM 186300), alternatively identified as Dowd type syndactyly, is a rare limb anomaly inherited in an autosomal dominant manner. Its main features include webbing of the ring and middle fingers, in addition to webbing of the 2nd and 3rd toes, coupled with a fusion of the 4th and 5th metacarpals (Ahmad *et al*., 2022).

Syndactyly type 6 (SD6)

SD6 (MIM 609432), also referred to as Mitten type, is a form of unilateral syndactyly. It is characterized by the webbing of all fingers in a hand except the thumb, along with fused 2nd and 3rd toes (Temtamy and Mckusick, 1978).

Syndactyly type 7 (SD7)

Characteristics of SD7 (MIM 212780) include 'disorganization' of phalangeal development, fusion of the metacarpals, and significant shortening of the ulna and radius (Cenani and Lenz, 1998). It is classified into syndactyly type V11-a and syndactyly type V11-b (Percin *et al*., 2003).

Syndactyly type VII-a

SD7a (MIM212780) recognized as "Cenani-Lenz type syndactyly" (CLS), with an autosomal recessive inheritance pattern. Phenotypically SD7a Individuals with severe hand deformities, encompassing all digital elements, display a distinctive cup-shaped

feature in SD7a. This characteristic is linked to the asymmetrical synostosis of phalanges, carpals, and metacarpals. (Niha, 2017).

Syndactyly type VIIb

SD7b, also known as the "Cenani–Lenz phenotype," is inherited in a dominant pattern. The phenotypic manifestations involve renal defects coupled with hearing impairment. The occurrence of SD7b is attributed to genomic rearrangements involving GREM1-FMN1 (Wang *et al.*, 1997).

Syndactyly type 8 (SD8)

SD8, recognized as "Orel-Holmes type" syndactyly, is identified by the fusion of the 4th and 5th metacarpals, accompanied by a noticeable ulnar deviation of the 5th digit and the absence of additional deformities. This syndactyly variant is characterized by shortened 4th and 5th metacarpals with evident separation between their distal ends, as reported by Jones et al. in 2014. The OMIM database categorizes this type as "Metacarpal 4–5 fusion" (MF4) (OMIM No. 309630).

Syndactyly type 9 (SD9)

SD9, referred to as "Mesoaxial synostotic syndactyly" (MSSD; OMIM No. 609432), has been documented in both a consanguineous Pakistani family and a consanguineous Turkish family. The discerned phenotypic characteristics include mesoaxial reduction of digits, metacarpal synostoses, clinodactyly, thumb hypoplasia, and partial or complete syndactyly of the toes (Malik *et al.*, 2005)

AIMS AND OBJECTIVES

The current study aim is to identify genetic variants in two Pakistani families with polydactyly and syndactyly respectively. This study also aims to develop a genotype and phenotype correlation among affected families. To achieve this objective, Whole Exome Sequencing (WES) of family A members was performed, and possible candidate genes were shortlisted using different bioinformatics tools and software, Homozygosity mapping of family B was performed and followed by conventional Sanger DNA Sequencing for confirming its segregation in the family. Using various online bioinformatics tools, the impact of the pathogenic variants was detected. This investigation holds the potential to contribute to the accurate diagnosis of genetic skeletal disorders and play a crucial role in providing genetic counseling to the affected family.

MATERIALS AND METHODS

Research Approval

Two families of syndactyly and Postaxial polydactyly (PAP) of Pakistani population were included in the present research study. The Institutional Review Board (IRB) of Quaid-i-Azam University Islamabad, Pakistan approved the current work. Affected members of the families and legal guardians of the affected family members provided written signed consents for genetic investigations.

Family's recruitment

Field survey of two families with Postaxial polydactyly and syndactyly phenotypes were conceded in the Khyber Pakhtunkhwa (KP) province and south Punjab, respectively. The research outcomes and future perspective were explained to the families who agreed to take part in this study. The recruited families were affected with Non-Syndromic PAP and syndactyly showing an Autosomal Recessive (AR) inheritance pattern. Photographs and previous medical records of affected family members were taken.

Pedigree Construction

Elder family members were interviewed, and pedigrees were designed using the concept by Bennett *et al*., 2008. Hollow circles and squares were used to represent unaffected females and males respectively while those with dark shading represented affected members. The crossline over the symbols represented deceased members. In pedigree, double horizontal lines indicate consanguineous marriage while vertical lines were used to indicate generation. Each consecutive generation was represented by a Roman number from top to bottom and its members were identified by Arabic numerals.

Blood sample collection

Blood samples from afflicted individuals, their parents and clinically normal siblings were collected by 10 ml syringes in EDTA tubes (BD Vacutainer K3 EDTA, Franklin Lakes NJ, USA). These samples of blood were then conserved at 4°C.

DNA Extraction

The manual phenol-chloroform technique and the commercially available kit were both used to extract the DNA. Before extraction, the blood samples were kept at 25°C (RT) for 20-30 min for its components to slightly settle down.

a. Phenol-chloroform method

- On day 1, we prepared an Eppendorf with 700µl of blood and 700µl of solution A, shake it 6-7 times, and let it sit at (RT) room temperature for 30 to 35 mins.

- Centrifuged the Eppendrof for about 1 minute at 13,000 rpm.

- at the bottom of the eppendor, pellet was formed which was further resuspended in 400µl solution A while discarding the supernatant.

- After discarding the unwanted supernatant, the remaining pellet, incubated overnight at 37°C with 450µl of solution B, 17µl of 20% SDS, and 13µl of proteinase K.

- On day 2, the Eppendorf containing the dissolved pellet was mixed with an equal volume (each 250µl) of Solution-C and Solution-D.

- After that tubes were centrifuged at a speed of 13,000rpm for 10 min. to form three distinctly distinguishable layers.

- Using a new Eppendorf, the topmost aqueous layer was proficiently transferred, mixed with 500µl of Solution-D and centrifuged once more for 10 min at 13,000rpm.

- The DNA-containing aqueous layer was collected in an autoclaved Eppendorf tube with 55µl sodium acetate and 450µl chilled isopropanol to precipitate out the DNA.

- To concentrate the DNA at the bottom of the tube, Eppendorf was centrifuged for 10 minutes at 13,000rpm. Supernatant was discarded and the DNA pellet again centrifuged at 13,000rpm for 7 minutes after being rinsed with 200µl of 70% ethanol.

- After centrifugation, any remaining ethanol was taken out and the pellet was dried using an Eppendorf vacuum concentrator ―5301" [Hamburg, Germany] for 15-25 minutes at 45°C.

- The dried-out DNA pellet diluted in 120-200µl Tris-EDTA (TE-Buffer) and stored at 4°C.

- Composition of the used solutions for DNA Extraction is shown in table 2.1.

Table 2.1: Composition of the solutions used for DNA Extraction

Solutions	Compositions
Solution A	Sucrose (0.32) + MgCl2 (5mM) + Tris. (10mM: pH 7.5) + 1% (v/v) Triton-X-100/
Solution B	EDTA (2mM:pH8.8) + NaCl (400mM) + Tris (10mM: pH7.5)
Solution C	Phenol
Solution D	Chloroform + Isoamyl Alcohol (24:1)
20% SDS	10g in 50 ml water.
70% Ethanol	70 l ethanol in 30 ml distilled water.

b. Extraction of DNA through the Kit Method

A commercial DNA extraction kit (Sigma-Aldrich, Gene Elute Blood Genomic DNA kit) was used to extract genomic DNA from blood.

- In a 1.5ml Eppendorf tube, 200µl of a whole blood sample, 200µl of lysis buffer, and 20µl of PK enzyme were homogenized together and were placed in a water-based bath to incubate around 55°C for 10 min.

- 200µl of 100% ethanol had been added, and the mixture was vortexed for 1520 seconds.

- The entire combination was poured into the mini-prep column and centrifuged for one min at 8000 rpm.

- The flow-through was eliminated, and then DNA was washed with 500µl of each wash buffer (WB1 & WB2) and centrifuged for 1-3 minutes at 8,000 13,000 rpm respectively.

- To remove the remaining washing buffers, an empty spin was performed at 13,000 rpm for 1 min.

- After washing, 250µl Elution Buffer was added and underwent incubation at 25°C for 10-15 minutes.

- Then, utilizing a high-speed centrifuge, DNA was extracted, placed in a tube, and stored at 4°C.

Agarose Gel Electrophoresis (1%)

To check the integrity and quality of DNA, Agarose Gel Electrophoresis was performed. For DNA visualization, 1% agarose gel was prepared. The composition of the gel is mentioned in Table 2.2. To generate a total volume of 100ml, 90ml of distilled water was mixed with 10ml Tris-Borate EDTA (TBE) also called 10X buffer solution. The solution was poured into a beaker and 1g of agarose powder was added after weighing. The DNA was then stained by adding 6 ml of ethidium bromide (EtBr) dye to the solution. The gel was transferred into a gel casting tray, where it was left to solidify for roughly 30 minutes. Afterwards, the gel was poured into an electrophoresis tank with 1X running buffer. DNA samples (3µl) were put into a gel along with an equivalent amount of loading dye (bromophenol blue) and the voltage was adjusted to 120 volts. The DNA strands were visualized using a UV trans-illuminator [Biometra, Gottingen, Germany].

Table 2.2: Description of solutions composition used in agarose gel electrophoresis

Chemicals	Composition
Agarose	0.5g
Ethidium Bromide	4µg/ml
TBE (10X) buffer	EDTA [0.032M: 8.3pH] + Boric ac id [0.025M] + Tris [0.89M]
Gel Loading Dye	Bromophenol blue dye [0.25%] + Sucrose [40%]

DNA Quantification and Dilution

The Colibri micro-volume spectrophotometer (Titertek Berthold, Germany) was used for the quantitative analysis of DNA and the readings were obtained at an optical density (OD) of 260 nm. First, the spectrophotometer was blanked and measured by using 2µl of TE buffer and then 2µl of DNA samples were loaded to measure their concentration in ng/µl units. Depending on DNA concentration, DNA was diluted to 20-30 ng/µl by adding PCR water.

Genotyping and Linkage Analysis

Microsatellite markers were used to search for homozygous regions underlying skeletal disorder in family A for the known loci and gene. The genetic distance between the microsatellite markers that surrounded these known loci, which were located using the UCSC genome browser. Five to ten microsatellite markers within centimorgans (cM) of the specific locus and gene were employed to confirm the homo and heterozygosity of these markers in affected and normal individuals.

After the detection of a convincing linkage to an already reported gene in any family, the gene of interest was Sanger sequenced to find out disease causing variant in respective family.

Whole Exome sequencing

DNA samples of about 3-5µl belonging to normal wild type and affected members of both families were subjected to WES at Yale Center for Genome Analysis (YCGA),

USA. The preparation of sequence libraries was accomplished by using IDT-xGen capture, USA. The sequencing proceedings were further carried out in the Illumina [HiSeq4000] platform. The reads of paired-end sequences were converted into FASTQ files and aligned with the human genome reference [hg.19] provided by UCSC. Various parameters of the alignment including quality recalibration, elimination of duplicated reads, variant detection, variant calling, and Indel realignments were evaluated through the Picard and Genome Analysis Toolkit (GATK), (Van der Auwera *et al.,* 2013).

Polyacrylamide Gel Electrophoresis (PAGE)

After amplification by PCR, the amplified product was separated using an 8% non-denaturing polyacrylamide gel electrophoresis (PAGE). For the preparation of a single polyacrylamide gel, a 50ml solution was required that was prepared by following the recipe listed in table 2.2. The gel solution was poured between 1.5mm distance apart plates and a comb were placed. Let the gel solidify and polymerize for about 35-40 minutes at room temperature. A thorough mix of amplified product and bromophenol blue (6µl) was done before the loading of samples. The gel was run in a vertical tank at 147- 155 volts for about 3 hours. For this electrophoresis process, 1X TBE buffer was used as a running buffer and visualized through a UV transilluminator (Biometra, Gottingen, Germany) by using Et. Br solution as staining gel. Photographs were captured by using DC 290 camera system (Kodak Digital Sciences, New York, USA).

Table 2.3: 8% Polyacrylamide Gel Composition (50 ml)

Chemical	Composition	Volume	Function
30% Acrylamide	29g of polyacrylamide + 1g of NN'-Methylenebisacrylamide (29:1 ratio)	13.5 ml	Cross linkage to make polymer (Polymerization)
10x TrisBorate EDTA	0.89 M Tris, 0.89 M Borate, 0.02 M EDTA	5 ml	Optimal conditions (maintaining pH)
10% APS	Ammonium persulphate	0.35 ml (350 μl)	For initiating polymerization (Catalyst)
TEMED	N, N, N', N' – Tetra Methyl Ethylene Diamine	0.025 ml (25 μl)	For free radicals stabilization
Distilled H2O		31.125 ml	To adjust total volume

Primer Designing

The designs of exon-specific primers were created by using online accessible tools. Few reliable and accessible online tools were utilized for primer designing such as Primer3 Plus https://www.bioinformatics.nl/cgi-bin/primer3plus/primer3plus.cgi, and Primer Blast https://www.ncbi.nlm.nih.gov/tools/primer-blast/. The fundamental parameters of the primers comprising GC content, annealing temperature (Tm), self-annealing primer dimer, and product size were examined and verified through PCR Primer Stats https://www.bioinformatics.org/sms2/pcr_primer_stats.html and UCSC In-silico PCR software https://genome.ucsc.edu/cgi-bin/hgPcr, respectively. The selection criteria of the primers were based on hits and those primers were shortlisted that displayed single gene hit through the software of Blast-like Aligning Tool (BLAT) http://asia.ensembl.org/Multi/Tools/Blast?db=core. The primer sequence of the genes is mentioned as under.

Table 2.4: Primer sequences involve in post-axial polydactyly and syndactyly

Genes	Primer Sequence [5′→3′]	Base Pairs	Product size
MEOX2 1F	CTGTCGCTTTTCCTCTTGCC	20	475bp
MEOX2 1R	CACCCGTTCTCCCAATCCT	19	
KIAA2013 1F	GTTTCAACCACCCCACCATC	20	181bp
KIAA2013 1R	CACGGAAGGAAATGCTGGAG	20	
MED12 41F	GAGCCTGGGATTGTGAGACT	20	205bp
MED12 41R	GGATTGGTAGAAGGGTGGGT	20	
HOXD12 1F	GATGTAGGCGGTGCTGAAAT	20	792bp
HOXD12 1R	CGGTTCACCTCCCCTTACAC	20	
HOX12 2.1 F	CTCTTGCCTGCGACCTTCA	19	690bp
HOXD12 2.1 R	CCAGGAGCAAGGAGAGTTGG	20	
HOXD12 2.2 F	CCTTGCTTTCCTCAGTCCCT	20	690bp
HOXD12 2.2 R	GGGGATCCAGTTACAGGGTT	20	

Pre-Sequencing PCR

The working principle of Polymerase Chain Reaction also known as PCR relies on the enzymatic amplification of sample DNA by targeting specific template sites. A 200µl PCR tube was utilized for the preparation of a total 25µl reaction mixture for amplification. The T3 Thermocycler (Biometra, Germany) was employed for the conduction of the PCR reaction.

About 1.5µl of DNA template, 0.7µl of each forward and reverse primer, 2.5µl of PCR buffer, 2µl of MgCl2, 0.7µl of dNTPs and 0.7µl of Taq polymerase, and 17µl of nuclease free water were the ingredients of the reaction mixture in the PCR tube. Following the loading of the PCR tube onto the thermocycler, amplification was carried out under the mentioned parameters.

Table 2.5: PCR conditions

PCR Stage	Temperature	Time Duration	Cycles
Initial Denaturation	96°C	7 minutes	
Final Denaturation	96°C	35 seconds	
Primer Annealing	54-64°C	30 seconds	
Initial Extension	72°C	35 seconds	30-35
Final Extension	72°C	7 minutes	
Hold	2-10°C	Pause	

Agarose Gel 2%

PCR products were analyzed on 2% agarose gel. 2g of agarose was added into 10 ml of 10X TBE and 90 ml of distilled water to prepare a 100 ml gel. The mixture was microwaved for about 2 minutes to dissolve the added ingredients. Then 6µl of Et.Br. was added to the mixture and poured into a gel tray to let it solidify for about 30 minutes. After solidification, the gel was transferred to a gel tank and PCR-amplified products were loaded along with 3µl of bromophenol blue dye. Electrophoresis was performed at 90 volts for about 45 minutes and bands were visualized by a gel doc UV analyzer.

Sequencing PCR products purification

Sequencing PCR products were purified by the Ethanol Precipitation Protocol (POP6 Protocol).

1) The products were put inside a 1.5 mL micro-centrifuge tube that consisted of 26 µl distilled water and 64 µl absolute ethanol. The products were then kept at 25°C for 10 min.

2) Centrifugation was done 13,000 rpm/20 min and the resultant supernatant was tossed away.

3) 250 µl 70% chilled ethanol supplied to the tubes.

4) The tubes were centrifuged again (13,000 rpm/10 min) after thorough mixing.

5) Supernatants were removed and 15 µl of Hi-Di Formamide, (HDF) was added for pellet re-suspension.

6) Mixture obtained was then placed in 0.5 ml septa tubes.

The purified products were then loaded onto a sample loading tray and preceded for sequencing through Automated Genetic Analyzer, ABI Prism 310® (Applied Biosystem USA).

Sanger Sequencing and Variant Annotation

The purified DNA of specific base pair size was then subjected to commercially available Sanger Sequencing and results were analyzed through the Bio-Edit Alignment software tool https://bioedit.software.informer.com/7.2/ . Chromatograms of affected and normal members were then analyzed with the reference sequence of genes obtained through the UCSC genome browser.

Table 2.6: List of Microsatellite Markers Used for Homozygosity Mapping

S. No	Targeted Gene	Locus	Markers	Centi-Morgan
I	*LRP4*	11p11.2	D11S4133	66
			D11S1290	67
			D11S1910	68
			D11S4109	69
			D11S2370	70
Ii	*BHLHA9*	17p13.3	D17S1840	1.3
			D17S1529	2.8
			D17S2118	4.5
			D17S654	6.6
			D17S1845	9.93
Iii	*LMBR1*	7q36.3	D7S104	182.84
			D7S2465	183.20
			D7S2423	185.38
			D7S54	185.0
			D7S98	187.32
Iv	*CKAP2L*	2q14.1	D2S1890	121.06
			D2S1889	122.08
			D2S1888	123.64
			D2S1896	125.18
			D2S2953	126.96

V	*CHST1*	11p11.2	D11S1290	67
			D11S4174	68
			D11S4109	69
			D11S2363	70.29
			D11S1764	71.56
Vi	*SMO*	7q32.1	D7S1874	130.7
			D7S461	131.1
			D7S530	133.1
			D7S649	135.7
Vii	*LAMA2*	6q22.33	D6S407	132.56
			D6S2437	133.46
			D6S1705	134.08
			D6S1572	135.46
			D6S1656	136.0
Viii	*SOST*	17q21.31	D17S760	67
			D17S1801	68.54
			D17S1860	69.7
			D17S579	69.9
			D17S810	70.65
Ix	*PAX3*	2q36.1	D2S126	225.6
			D2S2148	226.1
			D2S102	227.1

X	*EDNRB*	13q22.3	D13S162	71.71
			D13S782	72.84
			D13S1281	73.25
			D13S160	74.2
Xi	*RAB23*	6p12.1-p11.2	D6S294	81.8
			D6S1636	82.4
			D6S414	83.5
			D6S1695	84.2
			D6S1046	84.51
			D6S1551	85.64
Xii	*HOXD12*	2q31.1	D2S1274	182.9
			D2S2307	184.0
			D2S2314	185.6
			D2S2173	186.9
			D2S324	188.2
			D2S2310	188.9

RESULTS

Family A

Family A was recruited from District Bannu, KPK province of Pakistan. The pedigree shows a total of eight members, which includes two parents (I-1 and I-2) three affected individuals (II-3, II -4 and III-1) and three normal members (II-2, II-5 and II-6), that participated in the present study **(Figure 3.1)**.

Clinical features

All three affected individuals **(II-3, II -4 and III- 1)** of family A observed bilateral postaxial polydactyly type A. We assumed to be an autosomal recessive or X-linked recessive pattern as only males were affected. Only upper limbs were affected while lower limbs remained unaffected and did not show any other symptoms and anomalies that showed isolated post axial polydactyly type A **(Figure 3.2)**.

Genetic Investigation

DNA of affected members (II-3, II -4) and parents (I-1 and I-2) of family A were subjected to Whole Exome Sequencing. Analysis of the exome data filtered 46219 variants. To find out disease-causing variants in the Excel file in this regard various filters were applied. Focused only for pathogenic missense, non-synonymous, frame-shift and non-sense deletions/insertions. At first, only splice-site and exonic variants were selected for the homozygous genotype. In the second filter, the CADD Phred score of ≥ 13, allele frequency ≤ 0.005 was selected. For autosomal recessive one variant in one gene MEOX2 was shortlisted for the segregation analysis (Exon1:c .225_230del) which later on was not segregated in any member, for X-linked recessive two missense variants of two genes were shortlisted for segregation analysis WDR13 (exon2:c.C29T) and MED12 (exon41:c.G5873C). WDR13 did not show any segregation. A missense variant (c.G5873C:p.G1958A) in exon 41 in MED12 gene, located at x chromosome was present. The variant in the *MED12* gene was segregated through Sanger Sequencing in one affected member. For confirmation other members will be sent for sanger sequencing. The variant (c. G5873C) had a CADD Phred score of 21.

Family B

Family B was sampled from DG khan city of Punjab province, Pakistan. This is a four-generation pedigree with consanguineous marriages. The pedigree consists of a total of

25 members of which 23 were normal and 2 were affected (Figure 3.4). Affected members of the family segregated the disorder in autosomal recessive inheritance pattern. Clinical features of the afflicted individual revealed syndactyly of 4th and 5th toes. The affected members have no other symptoms. (Figure 3.4). For the genetic analysis, the blood sample of four members of the family was collected. This included two normal individual (IV-2) and (IV-3) in generation IV and two affected members (IV-4), and (IV-5) in the fourth generation.

Homozygosity Mapping

Family B DNA of four individuals including two healthy (I and II) and two afflicted individuals (III and IV) were tested using polymorphic microsatellite markers for linkage to the potential candidate genes that were previously reported to cause syndactyly. Those markers were selected that are present in close vicinity of the causative genes (Table 2.6 from methodology). Candidate genes included *LRP4* (11p11.2), *BHLHA9* (17p13.3), *LMBR1* (7q36.3), *CKAP2L* (2q14.1), *CHST1* (11p11.2), *SMO* (7q32.1), *LAMA2* (6q22.33), *SOST* (17q21.31), *PAX3* (2q36.1), *EDNRB* (13q22.3), *RAB23* (6p12.1-p11.2) and *HOXD12* (2q31.1). PCR was performed by using standard conditions and protocol and then the product was analyzed on 8% PAGE stained with Et.Br. and visualized on a UV Transilluminator (Biometra, Gottingen, Germany). By using a digital camera (EDAS 290) (Kodak, NY, USA) Photographs were taken to illustrate an exclusion or linkage to any gene/locus. Analysis of the allele pattern was based on the homozygous bands for affected individuals and the heterozygous band pattern for normal individuals.

Genotyping results analysis revealed a linkage of family to HOXD12 gene with cytogenetic location 2q31.1 (**Figure 3.5**). Marker in linkage interval were found in the homozygous state in both the affected members while heterozygous in unaffected members of the family. Marker D2S2173 (186.2 cM) flanked the linkage interval.

Sequencing of *HOXD12* Gene

Genotyping results illustrate family B linkage to the *HOXD12* gene which is located on q arm of chromosome 2 (2q31.1.) To identify pathogenic variants in coding and/or intron and exon borders, primers for all two coding exons and one intron were designed using Primer3, software (https://primer3.ut.ee/). Designed primer sequences are listed in (Table no of primers in methods). Sanger sequencing data of one coding exon and one non-coding intron analysis failed to reveal any pathogenic variant (Figure 3.5). The remaining coding exon will be analyzed for further analysis. If the remaining coding exon fails to reveal any pathogenic variant, then the family will be subjected for the whole exome.
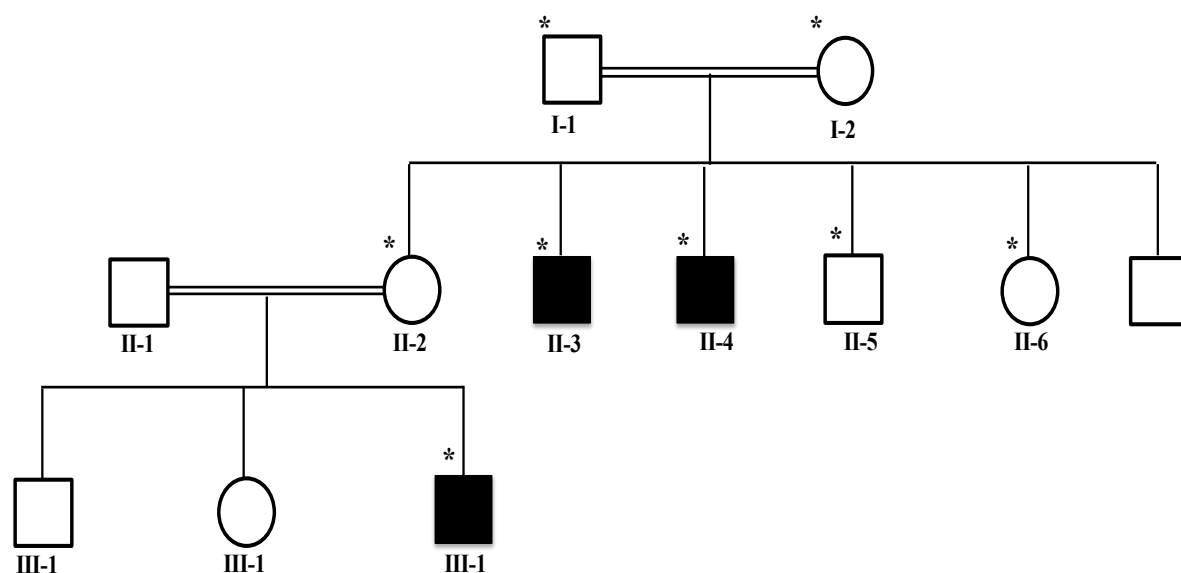
Figure 3.1: Pedigree of Family A shows an autosomal recessive, Or X-linked recessive inheritance pattern. Squares are used to show males, while circles indicate females. Black-filled shapes designate affected members whereas colorless shapes represent normal members. An asterisk (*) sign indicates sampled members. The double line between male and female indicates consanguinity. The crossline above the sample represents a deceased member. The generation position and family member's lineage are shown by Roman and Arabic numerals.

Figure 3.2: Clinical features of an affected member [II-3] of Family A, expressing postaxial polydactyly type

Table 3.1 Mutational analysis of MED12 gene in family A

Family ID	A
Gene	*MED12*
Nature of Mutation	Missense mutation
Mutation Detail	NM_005120: exon41:c.G5873C:p.G1958A
Status of Mutation	Novel Variant
No. of Hemi zygotes	8
Allele Frequency	0.00007156
CADD Score	21

Mutation Taster	Pathogenic
Varsome	Likely Pathogenic
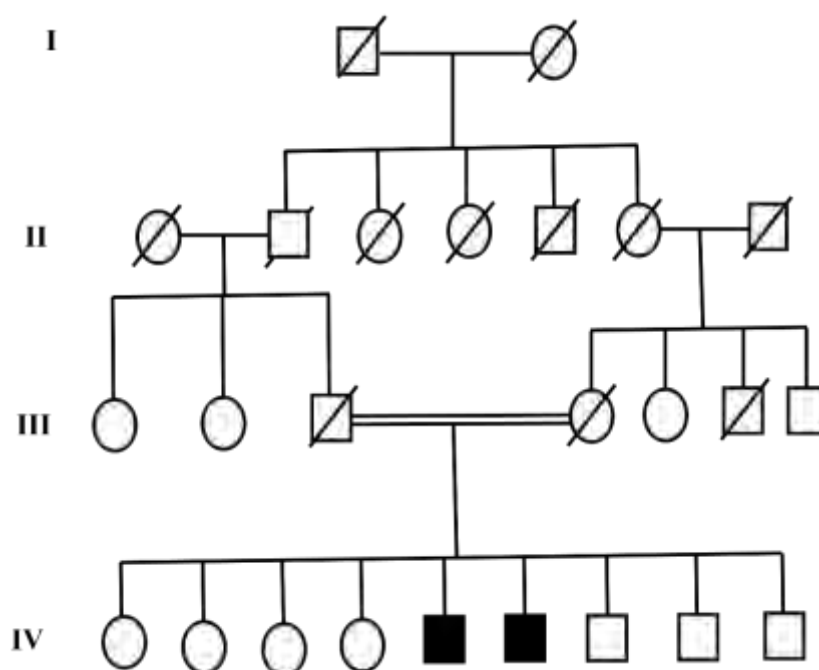
Figure 3.3 Pedigree of Family B shows an autosomal recessive, inheritance pattern. Squares are used to show males, while circles indicate females. Black-filled shapes designate affected members whereas colorless shapes represent normal members. An asterisk (*) sign indicates sampled members. The double line between male and female indicates consanguinity. The crossline above the sample represents a deceased member. The generation position and family member's lineage are shown by Roman and Arabic numerals.

Figure 3.4: Clinical features of an affected member of Family B expressing cutaneous syndactyly in 4th and 5th toes.
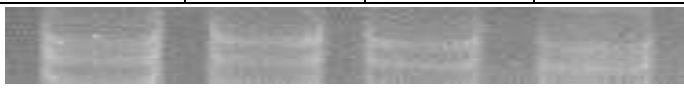
Genotyping Results of Family B
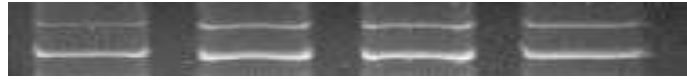
LRP4						
S.No	**Marker ID**	**Map Unit CM**	**N**	**N**	**A**	**A**
I	D11S4133	66				
II	D11S1290	67				
III	D11S1910	68				
IV	D11S4109	69				
V	D11S2370	70				
BHLHA4						
S.No	**Marker ID**	**Map Unit CM**	**N**	**N**	**A**	**A**
I	D17S1840	1.3				

Sequence Analysis of Candidate Genes Involved in Causing Bone Deformities in Consanguineous Families   39

II	D17S15 29	2.8				
III	D17S21 18	4.5				
IV	D17S65 4	6.6				
V	D17S18 45	9.93				
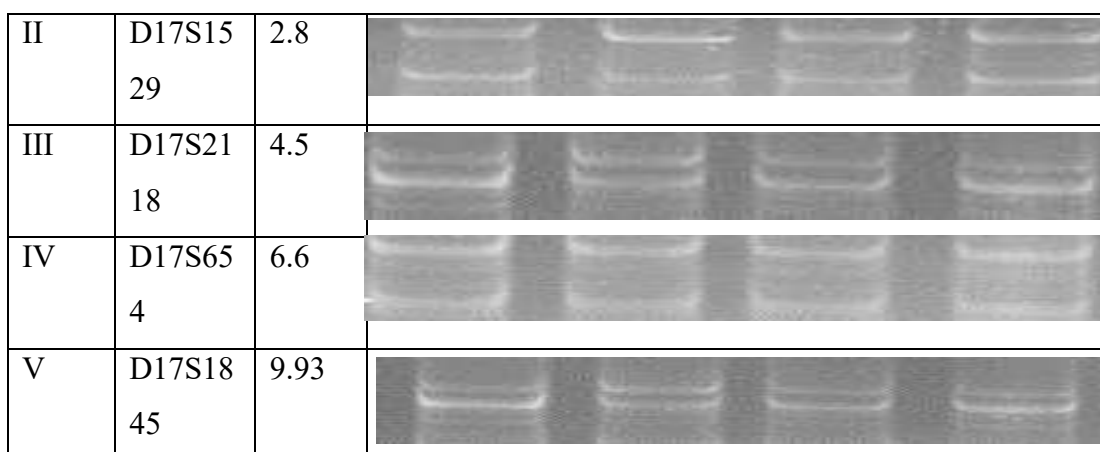
Figure 3.5: Polyacrylamide electropherogram illustrating the pattern of alleles amplified with specific microsatellite markers flanking *LRP4* and *BHLHA4* gene in family B. Roman and Arabic numbers indicate the generation position and number of individuals in a family pedigree.

LMBR1						
S.No	Marker ID	Map Unit CM	N	N	A	A
I	D7S104	182.84				
II	D7S2465	183.20				
III	D7S2423	185.38				
IV	D7S54	185.0				
V	D7S98	187.32				
CKAP2L						
S.No	Marker ID	Map Unit CM	N	N	A	A

Sequence Analysis of Candidate Genes Involved in Causing Bone Deformities in Consanguineous Families
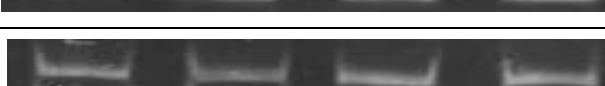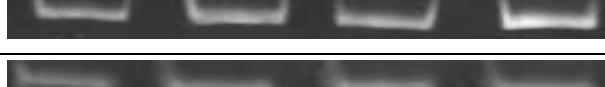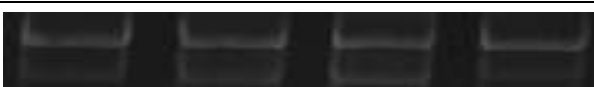
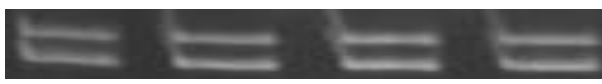| I | D2S1890 | 121.06 | |
Ii	D2S1889	122.08	
Iii	D2S1888	123.64	
Iv	D2S1896	125.18	
V	D2S2953	126.96	

Figure 3.6: Polyacrylamide electropherogram illustrating the pattern of alleles amplified with specific microsatellite markers flanking *LMBR1* and *CKAP2L* gene in family B. Roman and Arabic numbers indicate the generation position and number of individuals in a family pedigree.

CHST1						
S.No	**Marker ID**	**Map Unit CM**	**N**	**N**	**A**	**A**
I	D11S1290	67				
ii	D11S4174	68				
Iii	D11S4109	69				
Iv	D11S2363	70.29				
V	D11S1764	71.56				
SMO						
S.No	**Marker ID**	**Map Unit CM**	**N**	**N**	**A**	**A**
I	D7S1874	130.7				
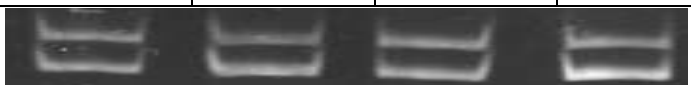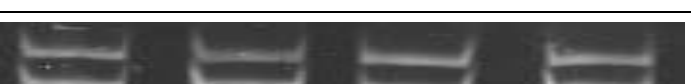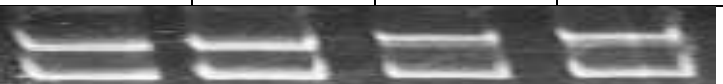
Ii	D7S461	131.1	
Iii	D7S530	133.1	
Iv	D7S649	135.7	

Figure 3.7: Polyacrylamide electropherogram illustrating the pattern of alleles amplified with specific microsatellite markers flanking *CHST1* and *SMO* gene in family B. Roman and Arabic numbers indicate the generation position and number of individuals in a family pedigree.
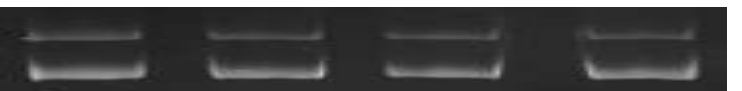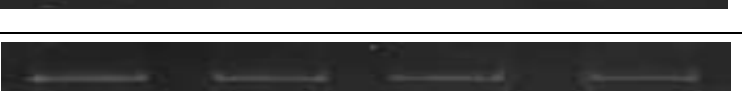
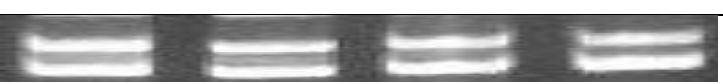| *LAMA2*						
S.No	**Marker ID**	**Map Unit CM**	**N**	**N**	**A**	**A**
I	D6S407	132.56				
ii	D6S2437	133.46				
Iii	D6S1705	134.08				
Iv	D6S1572	135.46				
V	D6S1656	136.0				
SOST						
S.No	**Marker ID**	**Map Unit CM**	**N**	**N**	**A**	**A**
I	D17S760	67				
Ii	D17S1801	68.54				

Iii	D17S1860	69.7	
Iv	D17S579	69.9	
V	D17S810	70.65	

Figure 3.8: Polyacrylamide electropherogram illustrating the pattern of alleles amplified with specific microsatellite markers flanking *LAM2* and *SOST* gene in family B. Roman and Arabic numbers indicate the generation position and number of individuals in a family pedigree.

PAX3						
S.No	Marker ID	Map Unit CM	N	N	A	A
I	D2S126	225.6				
ii	D2S2148	226.1				
Iii	D2S102	227.1				
EDNRB						
S.No	Marker ID	Map Unit CM	N	N	A	A
I	D13S162	71.71				
Ii	D13S782	72.84				
Iii	D13S1281	73.25				
Iv	D13S160	74.2				

Figure 3.9: Polyacrylamide electropherogram illustrating the pattern of alleles amplified with specific microsatellite markers flanking *PAX3* and *EDNRB* gene in family B. Roman and Arabic numbers indicate the generation position and number of individuals in a family pedigree.
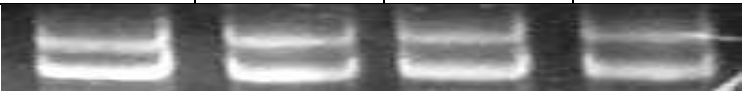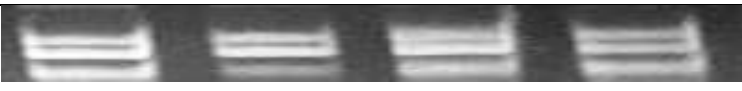
RAB23						
S.No	**Marker ID**	**Map Unit CM**	**N**	**N**	**A**	**A**
I	D6S294	81.8				
ii	D6S1636	82.4				
Iii	D6S414	83.5				
Iv	D6S1695	84.2				
V	D6S1046	84.51				
Vi	D6S1551	85.64				
HOXD12						
S.No	**Marker ID**	**Map Unit CM**	**N**	**N**	**A**	**A**
I	D2S1274	182.9				
II	D2S2307	184.0				
III	D2S2314	185.6				

Sequence Analysis of Candidate Genes Involved in Causing Bone Deformities in Consanguineous Families

IV	D2S324	188.2	
V	D2S2310	188.9	
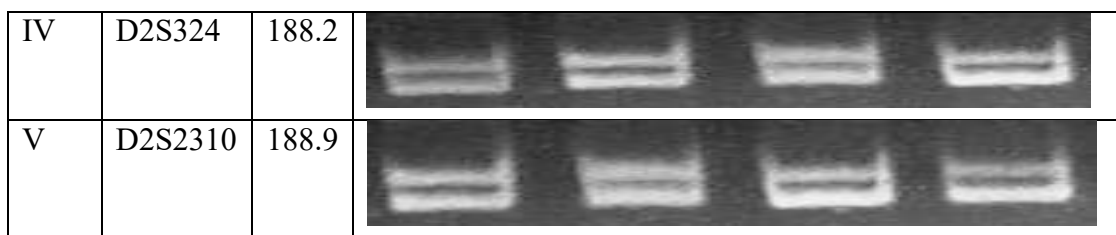
Figure 3.10: Polyacrylamide electropherogram illustrating the pattern of alleles amplified with specific microsatellite markers flanking *RAB23* and *HOXD12* gene in family B Roman and Arabic numbers indicate the generation position and number of individuals in a family pedigree.

S.No	Marker ID	N	N	A	A
I	D2S2173				
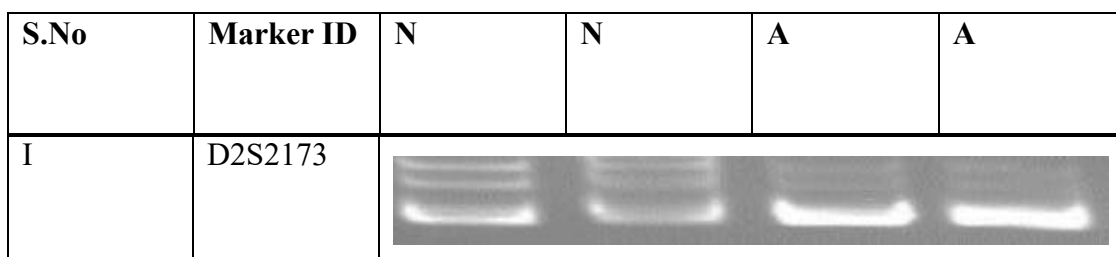
Figure 3.11 Polyacrylamide electropherogram illustrating homozygosity among the affected members of family B for microsatellite marker D2S2173 flanking the *HOXD12* gene on chromosome 2q31.1. Roman and Arabic numbers indicate the generation position and number of the members in a family pedigree.

Discussion

The skeletal system serves several essential functions, including supporting the body, protecting organs, facilitating linear growth, enabling mobility, and acting as a storage reservoir for minerals and blood cells (Krakow and Rimoin, 2010). The regulation of skeleton patterning and bone development involves close control by various transcription factors and signaling pathways associated with bone. Any mutation affecting these pathways or factors can disrupt the normal skeletal developmental process, resulting in Genetic Skeletal Dysplasia (GSD). In the Pakistani population, various disorders with patterns of autosomal dominant, recessive and X-linked have been identified, manifesting in both non-syndromic and syndromic forms. Notably, 82.5% of parents in different regions of Pakistan share a blood relationship, influenced by social, economic, religious, and cultural factors. All four of Pakistan's provinces have GSD cases on record. In Pakistan, there is a significant lack of attention given to rare genetic disorders such as GSDs. This issue is exacerbated by the country's ongoing challenges in providing sufficient genetic testing services. These conditions affect a small portion of the population, yet they can have an enormous impact on the lives of those affected. More resources must be devoted to addressing this issue and supporting those who need it (Umair *et al.,*2019).

Polydactyly, a genetic condition also known as 'Hexadactyly' is characterized by the additional digits on the hands or feet. This condition is inherited and can occur in varying degrees, ranging from a small skin tag to a fully formed extra finger or toe with bone, muscle, and nail. While it may not necessarily cause functional impairment, it can sometimes affect the normal development and movement of the affected limb. Polydactyly can be inherited in syndromic and non-syndromic forms. Non-syndromic polydactyly is further classified into Pre-axial, Post-axial, and Mesoaxial polydactyly.

Syndactyly is the most diverse developmental bone deformities documented in literature. Various types of combinations exist where adjacent fingers or toes connected each other by a web, allowing for unilateral/bilateral occurrences, as well as symmetrical or asymmetrical manifestations. Additionally, there is considerable phenotypic variability both within and between families. Condition is so

unpredictable that an individual may display dissimilar phenotypes in their upper and lower limbs or between the right and left sides. Syndactyly can be categorized as partial syndactyly or complete syndactyly, affecting either the skin or bones, and involving only phalanges or extending further to metacarpal/metatarsal or carpal/tarsal levels, and at times reaching distal end of the forearm/foreleg. On the milder end, a less severe phenotype may only be identifiable through changes in interphalangeal creases and unique dermatoglyphic features. Syndactyly can also be present as an isolated phenotype. There nine well-defined syndactylous entitie, the majority of which are non-syndromic. While most follow a Mendelian dominant inheritance pattern, there are descriptions of two autosomal recessive and one X-linked recessive type (Malik,2012).

The current research study aimed to characterize two Pakistani families having consanguineous marriages and identified with inherited post-axial polydactyly type B and syndactyly, respectively. These families were recruited from the remote areas of Khyber-Pakhtunkhwa (KPK) and south Punjab of Pakistan. To achieve the objective, blood samples were obtained from normal and affected members of the respective families for DNA extraction and further analysis.

In family A The individual's genome of the respective family was subjected to Whole Exome Sequencing for the determination of causative genetic variants involved in skeletal deformities. The exome data was further proceeded for analysis in the form of an Excel sheet and potential candidate variants were shortlisted. Candidate gene variants were selected based on their pattern of expression in bones or digits, skeletal growth, limb morphogenesis, and intricate molecular pathways governing limb development and growth. The shortlisted variants were analyzed and investigated for segregation analysis. Out of 46219 variants one variant for autosomal recessive (exon1: c.225_227del) of *MEOX2* and two variants for X linked recessive of *WDR13* (exon2: c.C29T) and *MED12* (exon41: c. G5873C) were shortlisted.

Both MEOX2 and WDR13 were not segregated by validation of Sanger DNA sequencing.However, one affected member of the family was segregated through Sanger sequencing of MED12 gene. Other remaining normal and affected will be further sequenced through Sanger sequencing to confirm segregation. In eukaryotes, the Mediator Complex is essential for initiating gene transcription. One of subunits of

Mediator Complex, Mediator of RNA polymerase II transcription subunit 12 homolog (MED12), controls the complex's activity. Numerous cellular processes include MED12, and mutations in the MED12 gene affect these processes and have been linked to a number of illnesses, such as prostate cancer, uterine leiomyomas, Opitz-Kaveggia syndrome, and Lujan syndrome. The biological role of MED12 and connection between MED12 mutations and diseases will be covered in this review. (Wang *et al*., 2013).

Family B was identified with 4th and 5th toes cutaneous syndactyly. On examination and investigation, none of the other symptoms were found in the affected members indicating isolated syndactyly. DNA samples of four individuals, two affected individuals (IV-3, IV-4), and two healthy (IV -2, IV -2) members were tested for homozygosity mapping by typing HPMM flanking the genes causing syndactyly. A minimum of 4 or 5 HPMM were selected for genotyping in the main region of known genes/loci. These genes included LRP4 (11p11.2), BHLHA9 (17p13.3), LMBR1 (7q36.3), CKAP2L(2q14.1), CHST1 (11p11.2), SMO (7q32.1), LAMA2 (6q22.33), SOST (17q21.31), PAX3 (2q36.1), EDNRB (13q22.3), RAB23 (6p12.1-p11.2) and HOXD12(2q31.1). One marker was linked to HOXD12(2q31.1).

Primers for both two exons and one intron region of HOXD12 were designed (**Table 2.4**). Sanger sequencing result of exon 2 and intronic region did not show any variant. Exon 1 is remaining, and it will be sequenced through Sanger sequencing. If exon 1 has been also cleared, then family B will be suggested for the whole exome for further investigation as reported genes are not involved and there might be a novel gene causing this phenotype.

REFERENCES

Agarwal P, Wylie J N, Galceran J, Arkhitko O, Li C, Deng C, Grosschedl R, Bruneau B G (2003). Tbx5 is essential for forelimb bud initiation following patterning of the limb field in the mouse embryo. Development 130; 623-633

Ahmad S, Ali M Z, Muzammal M, Mir F A, Khan M A (2022). The molecular genetics of human appendicular skeleton. Molecular Genetics and Genomics,297; 1195-1214.

Ahmad Z, Liaqat R, Palander O, Bilal M, Zeb S, Ahmad F, Jawad Khan M, Umair M (2023). Genetic overview of postaxial polydactyly: updated classification. Clin Genet 103; 3-15.

Akarsu AN, Ozbas F and Kostakoglu N (1997). Mapping of these condlocus of postaxial polydactyly type A (PAP-A2) to chromosome 13q21-q32. Am J Hum Genet 6; A265.

Altabef M, Tickle C (2002). Initiation of dorso-ventral axis during chick limb development. Mech Dev 116;19-27

Anderson BW, Ekblad J, Bordoni B (2018). Anatomy, appendicular skeleton. Europe PMC

Baldridge D, Shchelochkov O, Kelley B and Lee B (2010). Signaling pathways in human skeletal dysplasias. Annual review of genomics and human genetics 11; 189-217.

Castilla E, Paz J, Mutchinick O, Munoz E, Giorgiutti E and Gelman Z (1973). Polydactyly: a genetic study in South America. Am J Hum Genet 25; 405–412.

Cavalcanti DP, Fano V, Mellado C, Lacarrubba彗Flores MDJ, Silveira C, Silveira KC, Del Pino M, Moresco A, Caino S, Ramos Mejia R, Garcia CJ, Lay-Son G, Ferreira CR (2020). Skeletal dysplasias in Latin America. AJMG Part C 184; 986-995.

Chimal-Monroy J, Abarca-Buis R F, Cuervo R, Diaz-Hernandez M, Bustamante M, Rios-Flores JA, Romero-Suarez S, Farrera-Hernandez A (2011). Molecular control of cell differentiation and programmed cell death during digit development. IUBMB Life 63; 922-929.

Clarke B (2008). Normal bone anatomy and physiology. Clin J Am Soc Nephro 3;S131-S139.

Cole P, Kaufman Y, Hatef D A, Hollier L H Jr (2009). Embryology of the hand and upper extremity. J Craniofac Surg 20; 992-995.

De Baat P, Heijboer MP, de Baat C (2005). Development, physiology, and cell activity of bone. Ned Tijdschr Tandheelkd 112; 258-263.

Docherty B. Skeletal system: part four--the appendicular skeleton. Nurs Times (2007). Feb 20-26;103:26-7.

Duijf P H, van Bokhoven H, Brunner HG (2003). Pathogenesis of split-hand/split-foot malformation. Hum Mol Genet 12(suppl_1): R51-R60.

Elsner J, Mensah MA, Holtgrewe M, Hertzberg J, Bigoni S, Busche A, Coutelier M, de Silva DC, Elçioglu N, Filges I, Gerkes E (2021). Genome sequencing in families with congenital limb malformations. Hum Genet 140; 1229-1239.

ErlebacherA, Filvaroff EH, Gitelman SE, Derynck R(1995).Towards molecular understanding of skeletal development.Cell 80:371-378.

Galjaard RJH, Smits A, Tuerlings JH, Bais AG, Avella AMB, Breedveld G, Graaff ED, Oostra BA, Heutink P (2003). A new locus for postaxial polydactyly type A/B on chromosome 7q21– q34. Eur J Hum Genet 11; 409-415

Ghadami M, Majidzadeh-A K, Haerian BS, Damavandi E, Yamada K, Pasallar P, Najafi MT, Nishimura G, Tomita HA, Yoshiura KI, Niikawa N (2001). Confirmation of genetic homogeneity of syndactyly type 1 in an Iranian family. Am J Med Genet 104; 147–151

Guero S (2018). Developmental biology of the upper limb. Hand Surg Rehabil 37; 265-274.

Holmes LB, Nasri H, Hunt AT, Toufaily MH, Westgate MN (2018). Polydactyly, postaxial, typeB Birth defects research 110; 134-141

Hu J, He L (2008). Patterning mechanisms controlling digit development. J Genet Genomics 35; 517-524

Kalsoom UE, Klopocki E, Wasif N, Tariq M (2013). Whole exome sequencing identified a novel zinc-finger gene ZNF141 associated with autosomal recessive postaxial polydactyly type A. J Med Genet.50; 47- 53. doi: 10.1136/jmedgenet-2012-101219.

Klopocki E, Kähler C, Foulds N, Shah H, Joseph B, Vogel H (2012). Deletions in PITX1 cause a spectrum of lower-limb malformations including mirror-image polydactyly. Eur J Hum Genet 20; 705–708.

Kondoh S, Sugawara H, Harada N, Matsumoto N, Ohashi H, Sato M (2002). A novel gene is disrupte data14 q13breakpoint in a patient with mirror-image polydactyly of hands and feet. J Hum Genet 47; 136–139.

Kong X, Matise TC, Chen F, Chen W, De La Vega FM, Hansen M, He C, Hyland FC, Kennedy GC, Murray SS, Ziegle JS, Stewart WC, Buyske S (2007). A second generation combined linkage-physical map of the human genome. Genome Res 17; 1783-1786.

Kornak U, Mundlos S (2003). Genetic disorders of the skeleton: a developmental approach. Am J Hum Genet 73;447-474.

Krakow D, Rimoin DL (2010) .The skeletal dysplasias. Genetics in Medicine 12; 327-341.

Kumar D, Lassar A B (2014). Fibroblast growth factor maintains chondrogenic potential of limb bud mesenchymal cells by modulating DNMT3A recruitment. Cell Rep 8; 1419-1431

Lange A, Müller GB (2017). Polydactyly in development, inheritance, and evolution. Q Rev Biol 92; 1-38.

Lefebvre V (2019). Roles and regulation of SOX transcription factors in skeletogenesis. Curr Top Dev Biol 133; 171-193

Lefebvre V, Bhattaram P (2010). Vertebrate skeletogenesis. Curr Top De Biol 90: 29131

Malik S (2012). Syndactyly: phenotypes, genetics and current classification. Eur J Hum Genet 20; 817–24.

Malik S, Schott J, Ali SW, Oeffner F, Amin-ud-Din M, Ahmad W (2005). Evidence for clinical and genetic heterogeneity of syndactyly type I: the phenotype of second and third toe syndactyly maps to chromosome 3p21.31. Eur J Hum Genet13; 1268–74.

Malik S, Ullah S, Afzal M, Lal K and Haque S (2014).Clinical and descriptive genetic study of polydactyly a Pakistani experience of 313 cases/families. Clin Genet 85; 482–486.

Mallo M (2020). The vertebrate tail: a gene playground for evolution. Cell Mol Life Sci 77; 1021-1030.

Manske MC, Kennedy CD, Huang JI (2017). Classifications in brief: the Wassel classification for radial polydactyly. Clin Orthop Relat Res 475; 1740-1746.

Mariani F V, Ahn C P, Martin GR, (2008). Genetic evidence that FGFs have an instructive role in limb proximal-distal patterning. Nature 453; 401-405

Marin-Llera J C, Garciadiego-Cazares D, Chimal-Monroy J (2019). Understanding the Cellular and Molecular Mechanisms That Control Early Cell Fate Decisions During Appendicular Skeletogenesis. Front Genet 10; 977.

Montero J A, Hurle J M (2007). Deconstructing digit chondrogenesis. Bioessays 29; 725-737.

Montero J A, Lorda-Diez C I, Ganan Y, Macias D, Hurle JM (2008). Activin/TGFbeta and BMP crosstalk determines digit chondrogenesis. Dev Biol 321; 343-356

Namba N (2010). Genetic basis for skeletal disease. Nosology and molecular classification of skeletal dysplasias. Clin Calcium 20; 1159-1165.

Ng J K, Kawakami Y, Bü scher D, Raya A, Itoh T, Koth C M, Rodriguez Esteban C, Rodriguez-Leon J, Garrity D M, Fishman M C (2002). ThelimbidentitygeneTbx5promoteslimbinitiationbyinteractingwithWnt2band Fgf10. Development 129; 5161-5170.

Niha N (2017). Polydactyly—a review. Int J Inf Res Rev 04; 4302–4305

Oberg KC (2014). Review of the molecular development of the thumb: digit primera. Clin Orthop Relat Res 472; 1101-1105.

Palencia-Campos, A, Ullah A, Nevado J, Yildirim R, Unal E, Ciorraga M (2017). GLI1 inactivation is associated with developmental phenotypes overlapping with Ellis–Vancreveld syndrome Hum Mol Genet 26; 4556–4571

Pizette, Sandrine, Cory Abate-Shen, Lee Niswander (2001). BMP controls proximodistal outgrowth, via induction of the apical ectodermal ridge, and dorsoventral patterning in the vertebrate limb. Development 128;44634474.

Robson L and Syndercombe Court D (2018). Bone, muscle ,skin and connective tissue. In: Naish J , Syndercombe Court D (eds) Medical Sciences. London: Elsevier

Savarirayan R, Rimoin DL (2002). The skeletal dysplasias. Best Pract Res Clin Endocrinol Metab 16: 547-560.

Schrauwen I, Giese AP, Aziz A, Lafont DT, Chakchouk I, Santos⸎Cortez RL, Lee K, Acharya A, Khan FS, Ullah A, Nickerson DA (2019). FAM92A Underlies Nonsyndromic Postaxial Polydactyly in Humans and an Abnormal Limb and Digit Skeletal Phenotype in Mice. Journal of Bone and Mineral Research 34; 375-386.

Sparrow DB, McInerney-Leo A, Gucev ZS, Gardiner B, Marshall M, Leo PJ, Chapman DL, Tasic V, Shishko A, Brown MA, Duncan EL, Dunwoodie SL (2013). Autosomal dominant spondylocostal dysostosis is caused by a mutation in TBX6. Hum Mol Genet 22; 1625 1631.

Spranger J (2006). Skeletal dysplasias. In Human Malformations and Related Anomalies. Oxford University Press.

Stricker S, Mundlos S (2011). Mechanisms of digit formation: Human malformation syndromes tell the story. Dev Dyn 240; 990-1004.

Ullah A, Umair M, Majeed AI, Abdullah, Jan A, Ahmad W (2019). A novel homozygous sequence variant in GLI1 underlies first case of autosomal recessivepre⸎ axialpolydactyly. Clin Gen 95; 540-541.

Umair M, Ahmad F, Bilal M, Ahmad W, Alfadhel M (2018). Clinical genetics of polydactyly: an updated review. Front Genet 9; 447

Umair M, Palander O, Bilal M, Almuzzaini B, Alam Q, Ahmad F, Younus M, Khan A, Waqas A, Rafeeq MM, Alfadhel M (2021). The biallelic variant in DACH1, encoding Dachshund Homolog 1, defines a novel candidate locus for recessive postaxial polydactyly type A. Genomics 113; 2495-2502.

Umair M, Shah K, Alhaddad B, Haack TB, Graf E, Strom TM, Metiginer T, Ahmad W (2017). Exome sequencing revealed a splice site variant in the IQCE gene underlying post-axial polydactyly type A restricted to the lower limb. Eur J Hum Genet 25; 960-965.

Usami Y, Gunawardena AT, Iwamoto M, Enomoto-Iwamoto M (2015). Wnt signaling in cartilage development and diseases: lessons from animal studies. Lab Invest 96: 186-196.

WaldmannL, Leyhr J, Zhang H, Allalou A, Öhman፧MägiC, HaitinaT (2022).The role of Gdf5 in the development of the zebrafishfin endoskeleton.Developmental Dynamics,251; 1535-1549.

Wang CC, Chan DC, Leder P (1997). The Mouseformin (Fmn) Gene: Genomic Structure, Novel Exons, and Genetic Mapping. Genomics 39; 303–311.

Yu K, Ornitz D M (2008). FGF signaling regulates mesenchymal differentiation and skeletal patterning along the limb bud proximodistal axis. Development 135; 483-491

Zhao H, Tian Y, Breedveld G, Huang S, Zou Y, Chai J, Li H, Li M, Oostra BA, Lo WH, Heutink P (2002). Postaxial polydactyly type A/B (PAP-A/B) is linked to chromosome 19p13. 1-13.2 in a Chinese kindred. Eur J Med Genet 10; 162-166.

Sequence Analysis of Candidate Genes Involved in Causing Bone Deformities in Consanguineous Families